THE JOURNAL OF PHYSICAL CHEMISTRY C

pubs.acs.org/JPCC Article

Hydrogen Adsorption and Dissociation on $Al_nRh_2^+$ (n = 1 to 9) Clusters: Steric and Coordination Effects

Meiye Jia, Jan Vanbuel, Piero Ferrari, Wieland Schöllkopf, André Fielicke, Minh Tho Nguyen, and Ewald Janssens*

Cite This: J. Phys. Chem. C 2020, 124, 7624–7633 Read Online

ACCESS | Metrics & More | Article Recommendations | Supporting Information

ABSTRACT: The interaction of molecular hydrogen with doubly rhodium doped aluminum clusters, $Al_nRh_2^+$ (n = 1 to 9), is investigated by a combination of time-of-flight mass spectrometry, infrared multiple photon dissociation spectroscopy, and density functional theory calculations. The reactivity of the $Al_nRh_2^+$ clusters toward H_2 is found to be sensitive to cluster size, with sizes n = 1 to 4 and 7 being the most reactive. $Al_3Rh_2^+$ and $Al_4Rh_2^+$ are the only species that thermodynamically prefer molecular over dissociative H_2 adsorption. Calculated molecular adsorption energies of a single H_2 molecule correlate well with the experimental abundances of the hydrogenated species, and the potential energy profiles reveal that H_2 dissociation only has submerged barriers for n = 1, 2, and 7. In contrast, the molecularly hydrogenated complexes seem to be kinetically trapped for n = 5, 6, 8, and 9 due to significant energy barriers. This indicates that the initial molecular H_2 adsorption on the Rh atoms and thereafter dissociation are the determining steps for the hydrogenation reaction. An analysis of the cluster geometries reveals that the coordination environment and the steric factor of the Rh atoms are the main descriptors for the size-dependent reactivity of the $Al_nRh_2^+$ clusters.

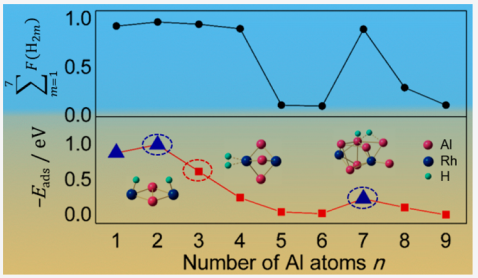

1. INTRODUCTION

Molecular hydrogen is considered a promising alternative for fossil fuels and already used at a small scale in the automobile industry.[1,2] One of the main challenges for the practical application of hydrogen as an energy carrier is its safe and efficient storage.[3] Many metal hydrides and complex hydrides, particularly aluminum based ones, have been investigated for the chemical storage of hydrogen.[4−6] Aluminum is light and abundant, but bulk aluminum is prone to oxidation and does not readily adsorb hydrogen. Transition metals are more efficient in activating H_2 under mild conditions.[7−10] Thus, it is of great interest to find aluminum-based alloys containing transition metals that are highly performant for the storage of hydrogen.

Study of the interaction of hydrogen with metal clusters under well-controlled conditions provides insight into the mechanisms involved in solid-state hydrogen storage.[11,12] Computations suggest that the low hydrogenation reactivity of most aluminum clusters can be attributed to a high activation barrier for the dissociation of the hydrogen molecule,[13] which can be reduced by alloying the clusters with transition metal atoms.[14] H_2 chemisorption on Al_nCo_m and Al_nNb_m bimetallic clusters was studied experimentally in a fast flow reactor in combination with mass spectrometry, and the observed composition dependent reactivity was hypothesized to be due to geometric and charge transfer effects.[15] Computationally, the interaction of H_2 with transition metal (M) doped aluminum clusters has been investigated for M = Sc, Y, Ti, V, Cr, Zr, Nb.[14,16−19] Those studies provided insight into the role of the dopant atoms in the H_2 adsorption, activation, and dissociation mechanisms. In general, the formation of hydrogenated metal clusters is initiated by molecular H_2 adsorption, followed by H_2 dissociation and H atom transfer.

Rhodium is an important catalyst for many reactions,[20,21] including hydrogenation prosseses.[22] Bulk Rh reacts strongly with molecular hydrogen and can dissociate hydrogen molecules.[23,24] At the nanoscale, the catalytic activity of rhodium can be further enhanced.[23] For example, it is reported that rhodium nanoparticles with diameters smaller than 10 nm exhibit hydrogen-storage capability.[9] In addition, the hydrogen adsorption capacity can be tuned by controlling the particle size. For few-atom Rh clusters, the hydrogen adsorption characteristics depend both on the precise cluster size and the adsorption site.[25−27] Recently, the interaction of H_2 with Rh doped clusters has been investigated, including $Al_{1-12}Rh^+$,[28] $Al_{10-13}Rh_2^+$,[29] and Mg_nRh (n = 1 to 10).[30] It was found that Rh doping significantly enhances the reactivity of aluminum and magnesium clusters toward hydrogen in a size-dependent way. Previous work by our group and by other researchers has demonstrated that addition

Received: December 3, 2019
Revised: March 7, 2020
Published: March 17, 2020

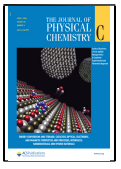

https://dx.doi.org/10.1021/acs.jpcc.9b11230
J. Phys. Chem. C 2020, 124, 7624–7633

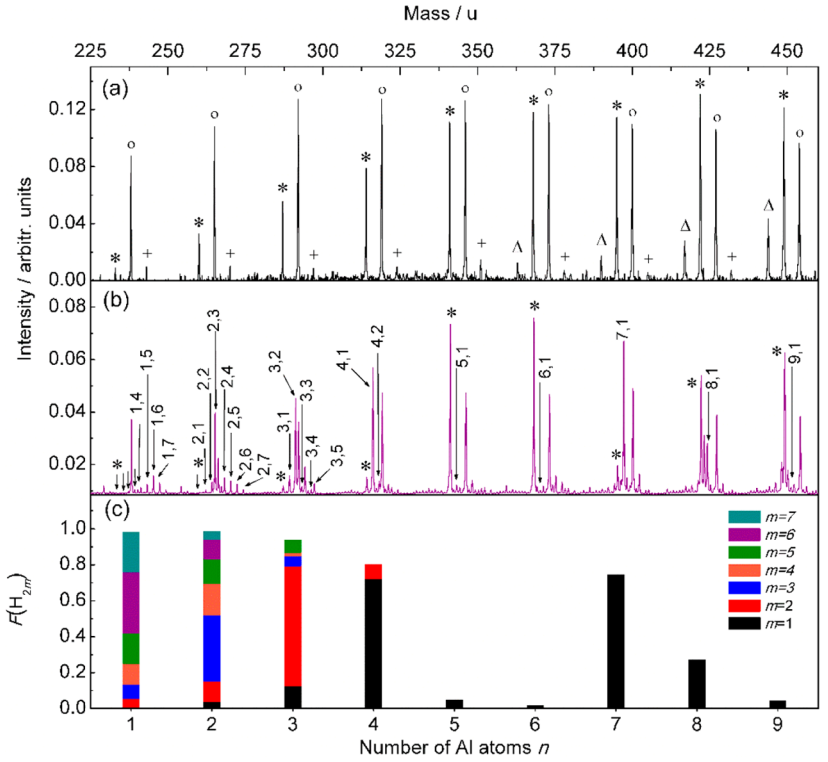

Figure 1. Mass spectra of (a) bare and (b) hydrogenated $Al_nRh_{1-3}^+$ clusters. (c) Fractions of hydrogenated clusters, $F(H_{2m})$, for $Al_nRh_2^+$ (n = 1 to 9). In parts a and b, peaks labeled with * correspond to bare $Al_nRh_2^+$ (n = 1 to 9) clusters. Additional peaks labeled in part a with the symbols °, Δ, and + are assigned to $Al_{5-13}Rh^+$, $Al_{2-5}Rh_3^+$, and Al_{9-16}^+ clusters, respectively. The (n, m) numbers in part b refer to $Al_nRh_2H_{2m}^+$. In part c, the fragments for hydrogenated n = 5−9 species with multiple H_2 ($m \geq 2$) are not given because of their negligible contributions.

of a second dopant atom can further enhance the reactivity of nanostructured materials toward hydrogen. Singly vanadium doped aluminum clusters, for example, are relatively inert toward hydrogen except for a few sizes,[14] whereas most of their doubly doped counterparts react with hydrogen under the same reaction conditions.[31] In a comparison of rhodium doped aluminum clusters of the same size, Al_nRh^+ and $Al_nRh_2^+$ (n = 10 to 12), the doubly doped species are more reactive toward hydrogen than the singly doped ones.[28,29] Similarly, Nonose et al. observed a gradual, monotonous increase in reactivity of cobalt doped aluminum clusters with an increase in the number of cobalt atoms.[15] Theoretical work by Chaudhuri et al. suggests that for the bulk metal hydride sodium alanate, the catalytically active site in the hydrogenation reaction consists of at least two neighboring Ti atoms.[32]

In previous work, we investigated the interaction of H_2 with singly Rh doped Al_nRh^+ (n = 1 to 12) clusters and found a significant size-dependent reactivity of Al_nRh^+, with n = 1 to 3 and 7 being the most reactive sizes. Furthermore, it was observed that H_2 favorably adsorbs molecularly on Al_2Rh^+ and Al_3Rh^+, while it prefers dissociative adsorption on the other studied sizes. The initial molecular adsorption of H_2 was identified as the determining step for hydrogenation of the Al_nRh^+ clusters, since the calculated molecular adsorption energies of H_2 correlate well with the experimental abundances of the hydrogenated clusters. In the current study, we use mass spectrometry, infrared multiple photon dissociation spectroscopy (IRMPD), and density functional theory (DFT) calculations to study the interaction of H_2 with a series of doubly Rh doped $Al_nRh_2^+$ (n = 1 to 9) clusters with the aim to further explore the cluster size dependency of a possible cooperative effect between the two dopant atoms.

2. METHODS

2.1. Experiments. The $Al_nRh_2^+$ (n = 1 to 9) clusters are produced in a dual-laser dual-target ablation source with rotating pure Al and Rh rods.[33] Helium carrier gas is introduced by a pulsed valve into the source, which is kept at room temperature, and initiates clustering of the ablated material. Molecular hydrogen is injected through a separate valve, located close to the nozzle of the source.[33] Expansion from the high-pressure region of the source into vacuum generates a beam of metal clusters and cluster-hydrogen complexes. The cationic particles are orthogonally extracted into a reflectron time-of-flight mass spectrometer. IRMPD spectra are obtained by scanning the wavelength of the free-electron laser (FEL) of the Fritz-Haber-Institut der Max-Planck-Gesellschaft[34] in the range of 800−2100 cm^{-1} (~50 mJ in a ~10 μs long pulse, 5−10 cm^{-1} fwhm bandwidth). The FEL is focused and overlapped with the cluster beam right before the clusters enter the extraction zone of the mass spectrometer. If the infrared light is in resonance with one of the IR active vibrational modes of the cluster-hydrogen complexes, multiphoton absorption takes place, heating up the cluster via internal vibrational redistribution.[35] When sufficient photons are absorbed, the cluster-hydrogen complex is fragmented and the intensity of that complex is reduced. The IRMPD cross section σ at a specific wavelength ν is calculated as

$$\sigma(\nu) = -\frac{\log(I/I_0)}{P(\nu)} \quad (1)$$

in which I and I_0 are the abundances of the hydrogenated complex in the mass spectrum with and without laser excitation, respectively, and $P(\nu)$ is the energy per pulse at that wavelength.

https://dx.doi.org/10.1021/acs.jpcc.9b11230
J. Phys. Chem. C 2020, 124, 7624−7633

2.2. Computations. DFT calculations are performed with the aid of the Gaussian 09 package[36] using the PBE exchange-correlation functional[37] in conjunction with the Def2-TZVP basis set.[38] This computational method performed well in our earlier studies of H_2 adsorption on single and double rhodium doped clusters, Al_nRh^+ (n = 1 to 12)[28] and $Al_nRh_2^+$ (n = 10 to 13).[29] The PBE functional was shown to be reliable for the properties of pure and doped aluminum clusters by comparison with CCSD simulations and experimental data.[39] Global optimizations are carried out for pure and hydrogenated $Al_nRh_2^+$ (n = 1 to 9) clusters whose initial guess structures are generated by the CALYPSO methodology.[40,41] The lower energy isomers of each species are collected and optimized for a range of possible spin multiplicities. For molecular and dissociative single H_2 adsorbed species, $Al_nRh_2{\cdot}H_2^+$ and $Al_nRh_2H_2^+$ (n = 1 to 9), a large number of structures are constructed and tested by adding one H_2 molecule or two H atoms to the lower energy isomers of $Al_nRh_2^+$. Various sites are considered for the H atoms (terminal, bridging, and facet) and the H_2 molecules (on both Al and Rh atoms). Harmonic vibrational frequency calculations confirmed that the obtained structures are minima on the potential energy surface and allow making zero-point energy (ZPE) corrections to the electronic energies. Reported relative energies are differences in Gibbs free energy at the source temperature of 298 K, $\Delta G_{298\ K}$. The calculated harmonic IR spectra are presented without any scaling. The D3 version of Grimme's dispersion correction with Becke-Johnson damping (GD3BJ)[42] is employed to include dispersion forces. The optimization of transition structures (TS) is performed using the Berny algorithm[43] from initial structures obtained through relaxed potential energy surface scans with appropriate internal coordinates. Vibrational frequency calculations are also performed to check that the reaction intermediates and transition structures have zero and only one imaginary frequency, respectively. Intrinsic reaction coordinate (IRC)[44] calculations are carried out to verify that each transition structure connects the two relevant local minima. Charge distributions have been analyzed on the basis of natural population analysis (NPA) as implemented in the Gaussian 16 package.[45]

3. RESULTS

3.1. Mass Spectra. Mass spectra of bare and hydrogenated $Al_nRh_2^+$ (n = 1 to 9) clusters are shown in parts a and b of Figure 1, respectively. The smallest clusters, $AlRh_2^+$ and $Al_2Rh_2^+$, are the most reactive species and adsorb up to seven H_2 molecules. For $Al_3Rh_2^+$, complexes with up to five H_2 molecules are detected. For the larger n = 4 to 9 sizes, the singly hydrogenated complexes dominate the observed abundances. Figure 1c shows the fractions of $Al_nRh_2H_{2m}^+$ (n = 1 to 9), which are obtained from the abundances (I) in the mass spectrum of Figure 1b by the expression

$$[F(H_{2m})] = \frac{I(Al_nRh_2H_{2m}^+)}{\sum_{i=0}^{7} I(Al_nRh_2H_{2i}^+)} \quad (2)$$

These fractions provide a quantitative means to assess the reactivity of the $Al_nRh_2^+$ (n = 1 to 9) clusters toward H_2. Sizes n = 1 to 4 and 7 are the most reactive species in the investigated size range, followed by n = 8. The n = 5, 6, and 9 clusters, in contrast, show very low reactivity. This distinct size-dependency is discussed in detail below.

3.2. Comparison of the IRMPD Spectra with Calculated IR Spectra. IRMPD spectra are recorded for the cluster-hydrogen complexes $Al_2Rh_2H_{2m}^+$ (m = 3 and 4), $Al_nRh_2H_4^+$ (n = 3 and 4), and $Al_nRh_2H_2^+$ (n = 4, 7, and 8). These are, for each n, the most abundant hydrogen complexes in the mass spectra. For n = 5, 6 and 9, the abundances of the hydrogenated complexes are too small to obtain spectra with a good signal-to-noise ratio. The experimental IRMPD spectra are compared in Figure 2 with

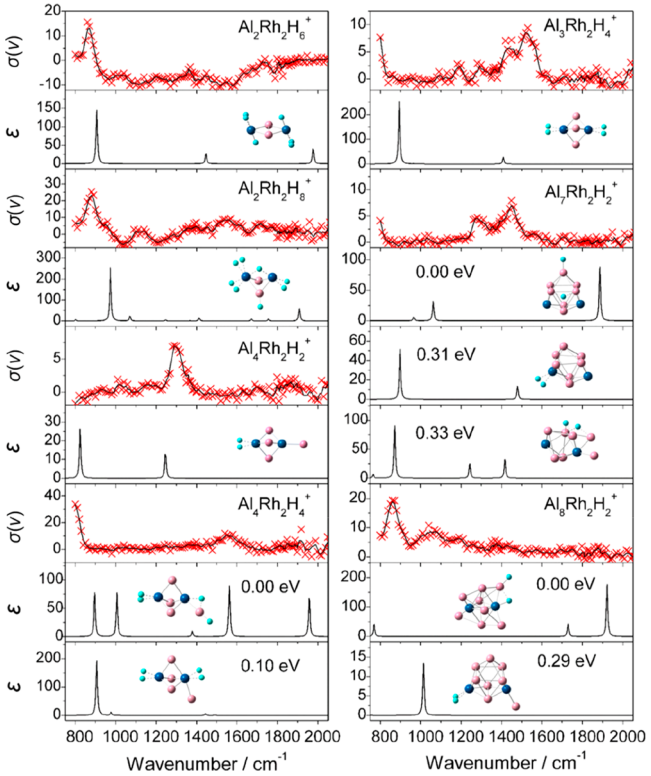

Figure 2. IRMPD spectra (top panels, the crosses are the original data points and the full lines correspond to three-point running averages) of $Al_2Rh_2H_{2m}^+$ (m = 3 and 4), $Al_nRh_2H_4^+$ (n = 3 and 4), and $Al_nRh_2H_2^+$ (n = 4, 7, and 8) and calculated IR spectra (bottom panels) of the corresponding lowest energy isomers. For $Al_nRh_2H_2^+$ (n = 7 and 8) and $Al_4Rh_2H_4^+$, the IR spectra of additional isomers are included. The reported relative energies are differences in Gibbs free energy at 298 K, $\Delta G_{298\ K}$. The experimental cross section $\sigma(\nu)$ and the calculated IR molar absorptivity ε are given in arbitrary units and M^{-1} cm^{-1}, respectively.

harmonic IR spectra for the computed lowest energy isomers and, where relevant, some additional low energy isomers. Infrared spectra of more isomers are given in Figures S1–S3 in the Supporting Information (SI). We note that calculated harmonic IR spectra are typically reliable to reproduce the number and the frequencies of the vibrational modes that are seen experimentally but are less accurate for predicting the relative intensities of those modes. The main reasons are the multiple photon aspect and the statistical dissociation of the cluster-hydrogens complexes in the experiment, which are not included in the computations.[46]

For $Al_2Rh_2H_6^+$, one intense broad band is observed in the IRMPD spectrum around 880 cm^{-1}. A comparison with the calculated IR spectrum of the lowest energy structure allows assigning this band to the symmetric stretches of two Rh–H_2 bonds. A similar spectrum is recorded for $Al_2Rh_2H_8^+$, showing a broad band around 890 cm^{-1} that is assigned to the symmetric

https://dx.doi.org/10.1021/acs.jpcc.9b11230
J. Phys. Chem. C 2020, 124, 7624–7633

stretching mode of Rh−H_2. The IRMPD spectrum of $Al_3Rh_2H_4^+$ shows an incompletely measured band around 790 cm^{-1} and one (or multiple) band(s) around 1400−1500 cm^{-1}. The calculated IR spectrum of the lowest energy structure, which has both H_2 molecules bound molecularly to Rh, agrees reasonably well with the experiment. The calculated symmetric and asymmetric stretching modes of the Rh−H_2 bonds are located at 893 and 1407 cm^{-1}, respectively.

For $Al_4Rh_2H_2^+$, only one band around 1300 cm^{-1} is discernible in the IRMPD spectrum. The calculated IR spectrum of the lowest energy structure, with molecular hydrogen attached to one of the Rh atoms, is consistent with the experiment. The calculated adsorption band at 1246 cm^{-1} agrees well with the measured band around 1300 cm^{-1}. The calculated Rh−H_2 symmetric stretching mode at 823 cm^{-1} may be outside the experimental spectral range. Also in our earlier study of $Al_nRhH_2^+$ (n = 1 to 12), the calculated harmonic Rh−H_2 symmetric stretching modes in the 800−900 cm^{-1} range seemed to be systematically blue-shifted compared to the experiment. This could partly be attributed to the particular anharmonic character of those vibrations.[28] As shown in Figure S16, the dissociation of the molecularly adsorbed H_2 requires overcoming an energy barrier of 0.67 eV ($\Delta G_{298\ K}$) with respect to the separated reactants $Al_4Rh_2^+$ and H_2. This suggests that the isomer detected in the experiment is the one with molecularly adsorbed H_2 and the dissociation is blocked by the energy barrier. The IRMPD spectrum of $Al_4Rh_2H_4^+$ shows one side of an intense band at 790 cm^{-1} and a weaker peak at around 1560 cm^{-1}. The calculated spectrum of the lowest energy isomer significantly differs from the measured IRMPD spectrum. A better agreement is found for an isomer located 0.10 eV above the ground-state structure, having one H_2 molecule attached to each of the Rh atoms. Considering the systematic blue-shift of the calculated Rh−H_2 modes, the calculated Rh−H_2 stretching mode at 905 cm^{-1} is in fair agreement with the measured band at around 790 cm^{-1}. The better agreement between the experiment and the calculation for the molecular H_2 adsorption state (0.10 eV isomer), suggests the existence of an energy barrier for H_2 dissociation in $Al_4Rh_2H_4^+$.

For $Al_7Rh_2H_2^+$, there is no agreement between the calculated harmonic IR spectrum of the lowest energy isomer and the IRMPD spectrum. The IRMPD spectrum shows no sign of an Al−H stretching mode around 1900 cm^{-1}. Instead, two higher energy isomers are able to reproduce the measured bands around 780, 1280, and 1440 cm^{-1}. One isomer (+0.31 eV) has the H_2 molecule bound to a Rh atom and has both symmetric and asymmetric Rh−H_2 vibrational modes at 898 and 1479 cm^{-1}, respectively. The other one (+0.33 eV) has both H atoms bound to Al−Al bridging sites with Al−H−Al vibrational modes at 871, 1243, and 1416 cm^{-1}. This indicates that for $Al_7Rh_2^+$, the calculated lowest energy isomer is not detected in the experiment. The calculations show a submerged barrier for the dissociation of H_2 on $Al_7Rh_2^+$ (Figure S25 in the Supporting Information). However, there could be barriers involved in the transfer of the H atoms from Rh to the Al sites to reach the lowest energy isomer. The experimentally probed species is likely a mixture of the molecularly hydrogenated isomer (+0.31 eV) and the isomer with dissociated hydrogen (+0.33 eV).

For $Al_8Rh_2H_2^+$, similar to $Al_7Rh_2H_2^+$, there is no agreement between the IRMPD and calculated IR spectrum of the lowest energy structure with dissociated hydrogen, because the calculated intense Al−H stretching mode at 1922 cm^{-1} is not observable in the IRMPD spectrum. Better agreement is found for an isomer (+0.29 eV) with H_2 adsorbed molecularly. As is shown in Figure S28, the H_2 dissociation on $Al_8Rh_2^+$ is characterized by an energy barrier of 0.79 eV ($\Delta G_{298\ K}$). The IRMPD spectrum has an intense band around 860 cm^{-1}, which could correspond to the calculated Rh−H_2 stretching mode at 1013 cm^{-1} (again significantly blue-shifted).

To conclude this discussion, even though exact structural assignment of the hydrogenated clusters is not possible by using only the recorded IRMPD data, it is possible to distinguish molecular from dissociative hydrogen adsorption. Interestingly, the presence of Al−H−Al bonds in $Al_7Rh_2H_2^+$ implies H_2 dissociation and spillover of H from the Rh dopants to the aluminum framework.

3.3. Calculated Structures of the Bare Clusters and the Cluster-Hydrogen Complexes. Figure 3 shows the optimized lowest-energy structures for the bare $Al_nRh_2^+$ (n = 1 to 9) clusters as well as molecular and dissociative single H_2 adsorption complexes, $Al_nRh_2{\cdot}H_2^+$ and $Al_nRh_2H_2^+$. The lowest energy structures prefer the lowest possible spin states, i.e., doublet for the odd electron systems (n = 2, 4, 6 and 8) and singlet for the even electron systems (n = 3, 5, 7 and 9), with the exception of a triplet state for $AlRh_2^+$. Additional isomers of $Al_nRh_2^+$, $Al_nRh_2{\cdot}H_2^+$, and $Al_nRh_2H_2^+$ are provided in Figures S4−S8 in the Supporting Information.

3.3.1. Structures of the Bare $Al_nRh_2^+$ (n = 1 to 9) Clusters. As is shown in the left column of Figure 3, the $Al_nRh_2^+$ (n = 1 to 3, 7, and 9) clusters have symmetric Rh atoms, which is not the case for n = 4 to 6 and 8. The two Rh atoms form a Rh−Rh bond for n = 1 and 2, while there is no such bond for n = 3 to 9. The coordination number of both Rh atoms increases with cluster size. In the smaller clusters $Al_nRh_2^+$ (n = 1 to 3), all Al atoms bind to both Rh atoms. The geometric configurations of $Al_4Rh_2^+$ and $Al_5Rh_2^+$ can be obtained by sequentially adding Al atoms to one of the Rh atoms in $Al_3Rh_2^+$. $Al_6Rh_2^+$ also is based on the structural motif as $Al_3Rh_2^+$ but with elongated Rh−Rh distance and the three additional Al atoms bound to bridge sites. The $Al_7Rh_2^+$ consists of a distorted tetrahedral pyramid, formed by five Al atoms, with the remaining Al atoms and the Rh atoms binding to this moiety by forming Al−Al and Rh−Al bonds. $Al_8Rh_2^+$ and $Al_9Rh_2^+$ are obtained by adding Al atoms on top of the Rh atoms in $Al_7Rh_2^+$, via single Rh−Al bonds. Because of the small energy differences (within 0.10 eV) between the most stable isomers of the bare $Al_nRh_2^+$ (n = 5 to 9) clusters, presented in Figure S4 in the Supporting Information, it is possible that multiple structural isomers coexist in the experiment.

3.3.2. Single H_2 Adsorption and Dissociation on $Al_nRh_2^+$ (n = 1 to 9) Clusters. Considering the cluster−hydrogen complexes with molecularly adsorbed H_2, $Al_nRh_2{\cdot}H_2^+$ (middle column in Figure 3), the H_2 molecule prefers to bind to one of the Rh atoms for all sizes. For sizes n = 1 to 3, 7, and 9 with two identical Rh atoms, only one structure of $Al_nRh_2{\cdot}H_2^+$ is presented for each size. While for sizes n = 4 to 6 and 8 with nonidentical Rh atoms, two structures are given corresponding to the H_2 molecule attached on each of the Rh atoms. For n = 4 to 5 and 8, the preferred adsorption site is the least coordinated Rh atom.

Figure 4 shows the calculated reaction pathways for single H_2 adsorption and dissociation on the smallest $AlRh_2^+$ and $Al_2Rh_2^+$ clusters. The intrinsic reaction coordinates (IRCs) and potential energy curves (PECs) are given in Figures S9−S12. As is shown in Figure 4a, H_2 dissociation happens barrier-free for $AlRh_2^+$ with the transition states lying lower in energy with respect to the intermediates before them. Note that a transition state

https://dx.doi.org/10.1021/acs.jpcc.9b11230
J. Phys. Chem. C 2020, 124, 7624−7633

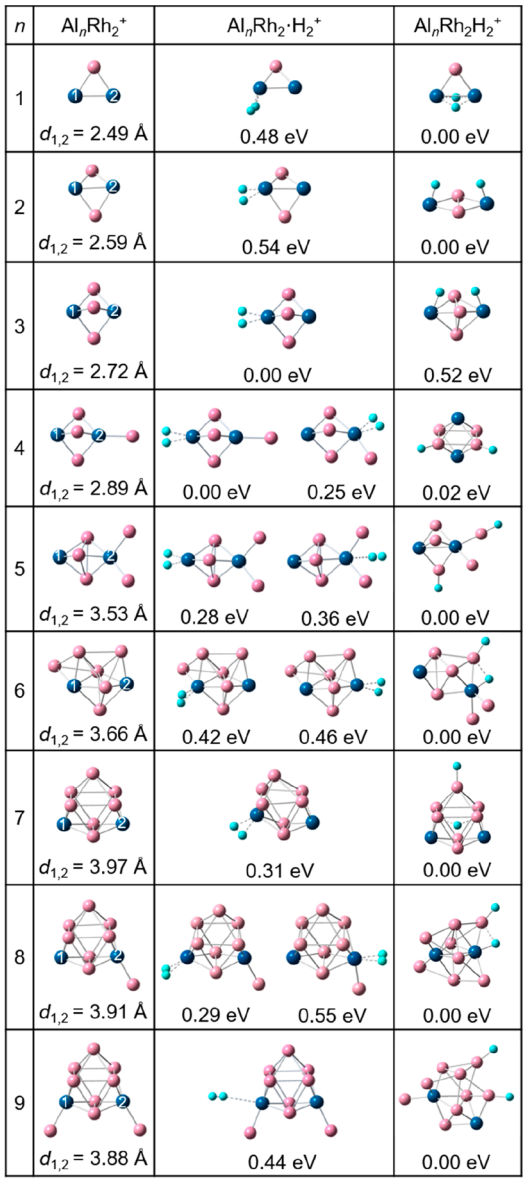

Figure 3. Optimized lowest energy structures of $Al_nRh_2^+$, $Al_nRh_2{\cdot}H_2^+$, and $Al_nRh_2H_2^+$ (n = 1 to 9). Blue, pink, and cyan spheres represent Rh, Al, and H atoms, respectively. For n = 4 to 6 and 8, the structures for H_2 adsorption on both Rh atoms are shown. The distances, $d_{1,2}$, of Rh−Rh bonds are shown for the bare $Al_nRh_2^+$ clusters. For the hydrogenated species, relative Gibbs free energies are given with respect to the lowest energy isomer.

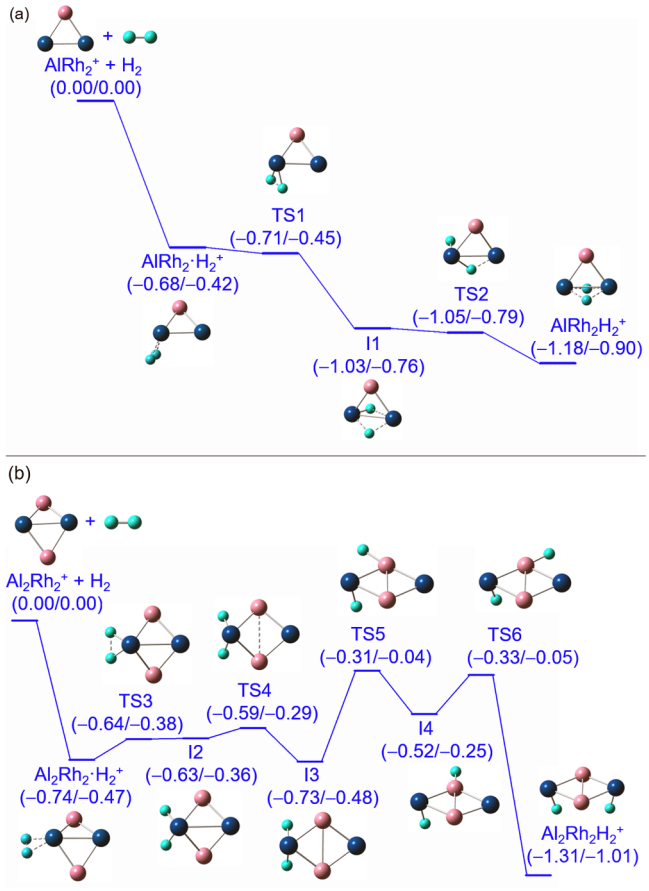

Figure 4. Calculated reaction pathways for the single H_2 adsorption and dissociation on $AlRh_2^+$ (a) and $Al_2Rh_2^+$ (b). The intermediates and transition states are denoted as In and TSn. Relative energies ($\Delta H_{0\,K}$/$\Delta G_{298\,K}$ in eV) are given with respect to the separated reactants, correspondingly.

should be higher in energy than its connecting intermediates, while the $\Delta G_{298\,K}$ energies of TS1 and TS2 are 0.03 eV lower than the intermediates ($AlRh_2{\cdot}H_2^+$ and I1) before them. This is due to the relatively high ZPE corrections to the energies of the intermediates under the formation of the Rh−H_2 ($AlRh_2{\cdot}H_2^+$) and Rh−H (I1) bonds. This phenomenon was also observed in the gas-phase reaction of manganese oxide cluster anions with hydrogen sulfide.[47] For interaction of H_2 with $Al_2Rh_2^+$ (Figure 4b), submerged barriers are encountered to reach the complex with dissociated hydrogen. All involved transition states are significantly lower (0.38, 0.29, 0.04, and 0.05 eV, correspondingly) in Gibbs free energy than the entrance channel ($Al_2Rh_2^+$ + H_2). Thus, the formation of the structure with dissociated hydrogen is both thermodynamically and kinetically favorable.

For the larger sizes (n = 3 to 9), the calculated energy profiles for single H_2 adsorption and dissociation as well as the related IRCs and PECs are shown in Figures S13−S32 in the Supporting Information. For those sizes, we calculated the barrier to dissociate the hydrogen starting from the molecular complex but not the entire energy profile to reach the lowest-lying structure, thereby ignoring other (possibly even higher) barriers for the migration of the hydrogen atoms to reach the lowest-energy structure. These (incomplete) energy profiles are sufficient to investigate possible kinetic trapping of the systems in the molecular adsorption state.

As shown in Figure S13 in the Supporting Information, the dissociation of the molecularly adsorbed H_2 on $Al_3Rh_2^+$ requires the overcoming of an energy barrier of 0.73 eV with respect to the separated reactants $Al_3Rh_2^+$ and H_2. In addition, the isomer $Al_3Rh_2{\cdot}H_2^+$, with molecularly adsorbed H_2, is thermodynamically more stable ($\Delta G_{298\,K}$ of −0.52 eV) than $Al_3Rh_2H_2^+$ with dissociated hydrogen. Therefore, it can be stated with confidence that H_2 adsorbs molecularly on $Al_3Rh_2^+$. Also on $Al_4Rh_2^+$ (Figure S16), H_2 dissociation suffers from energy barriers. The involved transition state is 0.93 eV higher than the molecular complex ($\Delta G_{298\,K}$ 0.67 eV above the entrance channel $Al_4Rh_2^+$ + H_2). In addition, the molecular complex has a lower Gibbs free energy (0.02 eV lower) than the complex with dissociated hydrogen, supporting the IRMPD observation of molecular H_2 adsorption. For $Al_5Rh_2^+$ and $Al_6Rh_2^+$ shown in

https://dx.doi.org/10.1021/acs.jpcc.9b11230
J. Phys. Chem. C 2020, 124, 7624−7633

Figures S19 and S22, the dissociation of the molecularly adsorbed H_2 suffers from high barriers of 0.67 and 0.41 eV, respectively, indicating that the molecularly adsorbed species are more likely to be detected in the experiment rather than the dissociative ones. Whereas for $Al_7Rh_2^+$, as is shown in Figure S25, the transition state is 0.21 eV lower in Gibbs free energy than that of the reactants $Al_7Rh_2^+ + H_2$. The small submerged barrier of 0.06 eV ($\Delta G_{298\ K}$) with respect to the molecular complex may hinder the dissociation of the hydrogen molecule, which could explain why we do not observe the most stable isomer in the experiment (Figure 2) but the molecular complex and a lower energy isomer with dissociated hydrogen (+0.33 eV). H_2 dissociation on $Al_8Rh_2^+$ (Figure S28) again suffers from an energy barrier which is 0.79 eV higher than the entrance channels ($Al_8Rh_2^+ + H_2$). Such a calculated barrier supports the IRMPD observation of molecular H_2 adsorption under the experimental conditions. For $Al_9Rh_2^+$, the H_2 molecule is weakly attached to one of the Rh atoms and it is repulsed by the cluster as it gets closer to the Rh atom (Figures S31 and S32 in the Supporting Information). This implies that it is even more difficult for the H_2 molecule to dissociate on $Al_9Rh_2^+$ even though the dissociative species has a lower Gibbs free energy.

Table 1 summarizes the calculated adsorption energies $-E_{ads}(H_2)$ and $-E_{ads}(2H)$ ($\Delta G_{298\ K}$ in eV) for molecular and dissociative H_2 adsorption, respectively. Also included are the H−H bond distances, d (H−H), and the Rh−H_2 distances, d (Rh−H_2), in case of molecular H_2 adsorption. The molecularly single H_2 adsorption on $Al_nRh_2^+$ clusters is exothermic, though the adsorption energy is very small for n = 5, 6, and 9. The molecular adsorption energies, $-E_{ads}(H_2)$, range from 0.02 to 0.47 eV, with values above 0.2 eV for n = 1 to 4 and 7. The high molecular adsorption energies for sizes n = 1 to 4 and 7, suggest the formation of Kubas complexes during the initial hydrogen adsorption process.[2] The H−H distances (0.79−0.89 Å) for n = 1 to 8 are elongated by 0.04−0.24 Å as compared to the bond length of the free H_2 molecule (d_{exp}(H−H) = 0.74 Å,[48] d_{calc}(H−H) = 0.75 Å at the PBE/Def2-TZVP level in this work), indicating an activation of the adsorbed H_2. For n = 9, the H−H bond distance (0.75 Å) is essentially the same as the bond length of the free H_2 molecule, indicating that H_2 is not activated in this case. For dissociative adsorption of a single H_2 molecule, $Al_nRh_2H_2^+$, the preferred adsorption sites for the H atoms strongly depend on the cluster size. In $AlRh_2H_2^+$, both H atoms are bound in a bridging configuration between the two Rh atoms, while in $Al_2Rh_2H_2^+$ and $Al_3Rh_2H_2^+$, each H atom is attached to one of the Rh atoms via a Rh−H bond. For n = 4, 5, and 9, both H atoms bind on top of an Al site. For n = 6 to 8, while one of the H atoms binds on top of an Al atom, the other binds at a Rh−Al (n = 6 and 8) or an Al−Al bridge site (n = 7). Note that the structures of $Al_nRh_2^+$ (n = 1 to 9) do not change noticeably upon molecular H_2 adsorption, while they do in the case of dissociative adsorption, in particular, for sizes n = 4, 6, 8, and 9.

Table 1. Adsorption Energies ($\Delta G_{298\ K}$ Values, Accounting for Entropic Effects) for Molecular [$-E_{ads}(H_2)$] and Dissociative [$-E_{ads}(2H)$] Adsorption of a Single H_2 Molecule on $Al_nRh_2^+$ (n = 1 to 9) Clusters. For the Molecular Complexes, also the H−H Distances [d(H−H)] and Rh−H_2 Distances [d(Rh−H_2)] are Given[a]

n	$-E_{ads}$(Rh−H_2)/ eV	d(H−H)/Å	d(Rh−H_2)/Å	$-E_{ads}$(2H)/eV
1	0.42	0.89	1.69	0.90
2	0.47	0.87	1.74	1.01
3	0.63	0.84	1.77	0.11
4	0.26/0.08	0.82/0.83	1.84/1.85	0.24
5	0.06/-0.02	0.79/0.76	2.01/2.52	0.29
6	0.04/0.01	0.82/0.79	1.87/1.98	0.46
7	0.27	0.86	1.76	0.58
8	0.12/-0.24	0.80/0.82	1.93/1.91	0.30
9	0.02	0.76	2.85	0.43

[a]In case of clusters containing asymmetric Rh atoms, values are provided for molecular H_2 adsorption on each Rh atom (see Figure 3), with the value before (after) the dash corresponding to that of the lower (higher) energy isomer.

The geometric structures and adsorption energies for the sequential hydrogen adsorption are analyzed for the smallest sizes n = 1 to 3. The lowest energy structures of $Al_nRh_2H_{2m}^+$ (n = 1 to 2, m = 2 to 7), $Al_3Rh_2H_{2m}^+$ (m = 2 to 5), and $Al_nRh_2H_{2m}^+$ (n = 4 to 9, m = 2) are given in Figures S33−S36 in the Supporting Information. The adsorption energies of the consecutive H_2 adsorption are tabulated in Table S2 in the Supporting Information. For $AlRh_2^+$, only the first two H_2 molecules are dissociatively adsorbed and the subsequent (m = 3 to 7) H_2 molecules are molecularly adsorbed on one of the Rh atoms. The adsorption energies tend to generally decrease with m, except for a maximum at m = 2. For $Al_2Rh_2^+$, as many as five H_2 molecules can be adsorbed and three of them are dissociated. The adsorption energies decrease with the increment of the number of attached H_2 molecules. For $Al_3Rh_2^+$, up to five H_2 molecules can be adsorbed of which only two H_2 molecules are dissociated. The adsorption energies evolve nonmonotonously with m.

The calculations reveal that both molecular and dissociative single H_2 adsorptions are thermodynamically and kinetically feasible for $AlRh_2^+$ and $Al_2Rh_2^+$; however, the dissociative adsorption is thermodynamically favored. For $Al_3Rh_2^+$ and $Al_4Rh_2^+$, molecular adsorption is thermodynamically favorable; furthermore, dissociation of H_2 is hindered by an energy barrier. In the case of n = 5, 6, 8, and 9, though the dissociative adsorption states have lower Gibbs free energies than the molecular adsorption states, they are kinetically difficult to reach due to considerable energy barriers. The presence of molecular H_2 adsorbed complexes for n = 4 and 8 are supported by comparisons of the IRMPD spectra of $Al_4Rh_2H_2^+$ and $Al_8Rh_2H_2^+$ to the corresponding calculated IR spectra. For n = 7, from the comparisons of the IRMPD and the calculated IR spectra for $Al_7Rh_2H_2^+$ in Figure 2, the calculated IR spectrum of the dissociative isomer 0.33 eV higher in energy (the two H atoms are bond at bridging sites) agrees better with the IRMPD than that of the molecular isomer (0.31 eV higher). Furthermore, the dissociation of the H_2 occurs almost barrier-free (Figure S25). So, it is likely that the 0.33 eV higher isomer is the one that is detected in the experiment, while the lowest energy dissociative isomer (0.00 eV) cannot be reached due to energy barriers involved in the transition of the two H atoms rather than the dissociation of the H_2.

As is shown in Figure 5, the fractions $\sum_{m=1}^{7} F(H_{2m})$ of the hydrogenated clusters in the experiment (part a), which represent the size-dependent reactivity toward hydrogen, are strongly correlated with the calculated molecular adsorption energies, $-E_{ads}(H_2)$ (panel b). In part c, the calculated dissociative energies, $-E_{ads}(2H)$, are adopted for $AlRh_2^+$, $Al_2Rh_2^+$, and $Al_7Rh_2^+$ (+0.33 eV isomer), while $-E_{ads}(H_2)$ energies are used for the other sizes. The energies in part c are

https://dx.doi.org/10.1021/acs.jpcc.9b11230
J. Phys. Chem. C 2020, 124, 7624−7633

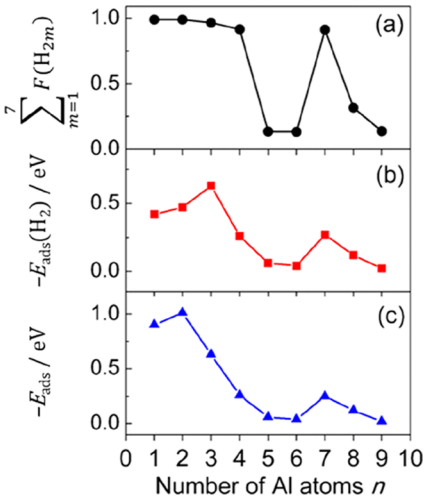

Figure 5. Comparison of (a) the total abundances, $\sum_{m=1}^{7} F(H_{2m})$, of $Al_nRh_2H_{2m}^+$ (n = 1 to 9) with the calculated adsorption energies ($\Delta G_{298\ K}$) for (b) molecular single H_2 adsorption on $Al_nRh_2^+$ (n = 1 to 9) and (c) preferred adsorption type for different sizes (dissociation for n = 1, 2, and 7 and molecular for n = 3 to 6, 8, and 9).

uniformly denoted as $-E_{ads}$ for clarity. The good correlation between $\sum_{m=1}^{7} F(H_{2m})$ and $-E_{ads}(H_2)/-E_{ads}$ suggests that the initial molecular H_2 adsorption is the key step for H_2 interaction with $Al_nRh_2^+$ (n = 1 to 9) clusters and the molecular H_2 adsorption complexes are those detected in the experiment for n = 3 to 6, 8, and 9, while dissociative single H_2 adsorption is preferred by the smallest clusters, $AlRh_2^+$ and $Al_2Rh_2^+$. For $Al_7Rh_2^+$, complexes with molecular and dissociative hydrogen may coexist. Considering the calculated molecular and dissociative adsorption energies (Table 1) and the possibility to dissociate molecularly adsorbed H_2 on $Al_nRh_2^+$ clusters (Figures 4, S9−S32), it can be concluded that the dissociation of molecular adsorbed H_2 is the rate-determining reaction step.

4. DISCUSSION

Details of both the geometric structure and electronic properties of small clusters are expected to be important for the reactivity toward H_2.[49−53] Correlations of the reactivity with ionization energies or electron affinities were found and explained by a charge-transfer model.[51,52] In the current work, a strongly size-dependent reactivity of $Al_nRh_2^+$ clusters toward H_2 is observed, with n = 1 to 4 and 7 being the most reactive sizes. In view of the correlation between the calculated H_2 adsorption energies with the abundances of the hydrogenated clusters (Figure 5), the molecular H_2 adsorption state is identified as the final product for sizes n = 3 to 6, 8, and 9 or as the rate-determining step for sizes n = 1, 2, and 7. For n = 1 and 2, the molecular H_2 adsorption states essentially provide the H_2 molecule energy and time to probe the potential energy surfaces for possible dissociation pathways. Energetically stable molecular H_2 adsorption states have also been observed in reactions of transition metal clusters M_n (M = Fe, Co, Ni, and W) with H_2/D_2.[53] In order to elucidate the size-dependent reactivity of $Al_nRh_2^+$ toward H_2 adsorption, the coordination of the Rh dopants, the charge distributions within the clusters, and the charge transfer between $Al_nRh_2^+$ and the adsorbed H_2 molecule are analyzed.

4.1. Steric and Coordination Effects. Table 2 summarizes the natural population analysis (NPA) charge distributions and coordination numbers (CN) of the two Rh atoms in $Al_nRh_2^+$ (n = 1 to 9) as well as the charge distributions of the two Rh atoms and the H_2 molecules in $Al_nRh_2{\cdot}H_2^+$ (for the case of single H_2 molecular adsorption). The CN of the two Rh atoms in $Al_nRh_2^+$ clusters gradually increases with the growing of cluster size; the Rh atoms become partially surrounded by Al. Generally, higher reactivity is identified for the bare clusters in which at least one Rh atom is low coordinated (CN = 2 to 4) and not shielded by the Al framework, namely, sizes n = 1 to 4 and 7. Lower reactivity is observed for the other sizes (n = 5, 6, 8 and 9), with one or two highly coordinated (CN = 5) Rh atoms and at least one of the Rh atoms partially encapsulated by Al atoms. Therefore, the geometric locations and coordination numbers of the Rh atoms seem to play decisive roles in determining the adsorption site of the H_2 molecule.

Table 2. Calculated NPA Charge Distributions [q(Rh)] and Coordination Numbers [CN] for both Rh Atoms in $Al_nRh_2^+$ (n = 1 to 9) Clusters, as well as the Charge Distributions [q(Rh)−H_2 and $q(H_2)$], for the Rh Atom and H_2 Molecule in $Al_nRh_2{\cdot}H_2^+$ (Values from PBE/Def2-TZVP Computations)

n	q(Rh)/e	CN	q(Rh)−H_2/e	$q(H_2)$/e
1	0.051	2	−0.213	0.150
2	−0.435	3	−0.777	0.164
3	−1.080	3	−1.587	0.236
4	−1.114/−2.269	3/4	−1.512/−2.297	0.186/0.253
5	−0.987/−2.886	3/5	−1.267/−2.926	0.120/0.024
6	−1.849/−1.221	5/4	−2.308/−1.588	0.240/0.158
7	−1.260	4	−2.068	0.288
8	−1.192/−2.418	4/5	−1.614/−2.439	0.172/0.223
9	−2.306	5	−2.312	0.027

4.2. Charge Distribution and Transfer. As shown in Table 2, the NPA charges on the Rh atoms in $Al_nRh_2^+$ clusters generally get more negative with increasing cluster size. Electron transfer occurs from H_2 to $Al_nRh_2^+$, and the charge on the Rh atoms becomes more negative than that in the bare $Al_nRh_2^+$ clusters. Figure 6 shows the electron density difference maps for the initial molecular H_2 adsorption on $Al_nRh_2^+$ (n = 1 to 9) clusters. For those sizes with nonidentical Rh atoms (n = 4 to 6

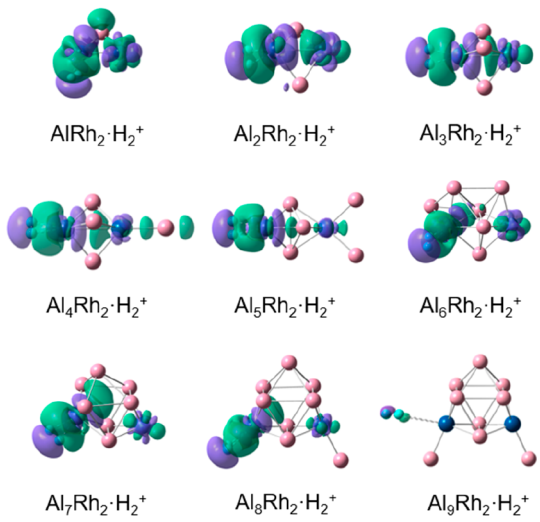

Figure 6. Electron density difference maps for H_2 molecular adsorption on $Al_nRh_2^+$ (n = 1 to 9). The green and violet isosurfaces (+0.001 and −0.001 au, respectively) represent regions in which the electron density is increased and decreased after formation of the complex, respectively. Values are from PBE/Def2-TZVP computations.

https://dx.doi.org/10.1021/acs.jpcc.9b11230
J. Phys. Chem. C 2020, 124, 7624−7633

and 8), only the lowest energy complexes are presented. For sizes n = 1 to 8, complex formation leads to significant increment of the electron density in the region between the H_2 molecule and the Rh adsorption site. This indicates that electron density shifts from the cluster and the H_2 molecule toward the region between them to enhance the interaction of the clusters with the H_2 molecule. Furthermore, for n = 1 to 4 and 7, the electron density also shows a significant increase inside the clusters, corresponding to Rh−Al or Al−Al interactions. For sizes n = 5 to 6 and 8, instead, the electron density increases slightly inside the clusters. For the interaction of $Al_9Rh_2^+$ with H_2, there is no effective charge transfer between the cluster and the H_2 molecule to facilitate the interaction. Thus, the interaction of $Al_9Rh_2^+$ with the H_2 molecule is very weak. This size-dependent charge transfer trend is consistent with the calculated molecular H_2 adsorption energies (Table 1) and it is very similar to the case for H_2 adsorption on singly Rh doped Al_nRh^+ (n = 1 to 12) clusters.[28] However, for the doubly Rh doped $Al_nRh_2^+$ (n = 1 to 9) clusters, the other Rh atom in $Al_nRh_2{\cdot}H_2^+$ is still accessible for additional H_2 adsorption, especially for those sizes n = 1 to 3 in which there are appreciable electron density changes on the unoccupied Rh atom. Thus, the second Rh atom acts either as an additional active site for further H_2 adsorption or as a promoter to facilitate the charge transfer during the process for H_2 adsorption on the first Rh atom.

4.3. Comparisons with the Singly Rh Doped Clusters.

In our previous work about H_2 adsorption on singly Rh doped Al_nRh^+ (n = 1−12) clusters,[28] a size-dependent reactivity was found, with sizes n = 1 to 3 and 7 being the most reactive. This was mainly attributed to the location of the Rh atom, with minor contributions coming from charge transfer effects. For the doubly Rh doped $Al_nRh_2^+$ (n = 1 to 9) clusters studied in this work, similarly, the reactivity is strongly size-dependent, with sizes n = 1 to 4 and 7 being the most reactive ones. Calculations revealed that the initial molecular adsorption of H_2 is mainly controlled by the coordination and a steric effect (the coordination number of Rh atoms and whether the Rh atoms are shielded or not). The charge transfer between cluster and H_2 plays an important role to stabilize the hydrogenated complexes. The energy barriers involved in H_2 dissociation determine whether the molecularly or dissociatively hydrogenated complexes are detected in the IRMPD experiment. In addition, the total charges on the Rh atoms, the E_{VIE} and E_{VEA} of the bare clusters, have minor influences on the size-dependent reactivity of $Al_nRh_2^+$ (n = 1 to 9) clusters, as shown (Figure S37 in the Supporting Information) for their correlation with the total abundances of the hydrogenated species.

For the singly Rh doped clusters, as many as four H_2 molecules can be attached to the small sizes n = 1 to 3, and nearly all are bound dissociatively. For the doubly Rh doped clusters, instead, five to seven hydrogen molecules are adsorbed for n = 1 to 3, with most of the hydrogen adsorbed molecularly. The enhanced hydrogen capacity of $Al_nRh_2^+$ (n = 1 to 9) clusters can be attributed to the second Rh atom which acts as an additional reactive site. From this point of view, it can be confirmed that the Rh atoms are the reactive center for initial molecular hydrogen adsorption and the number of the Rh dopant atoms in the clusters determines the H_2 adsorption capacity. Therefore, it is the number of the active Rh atoms that makes the difference for the reactivity of the singly and doubly Rh doped Al_nRh^+ and $Al_nRh_2^+$ clusters. Nevertheless, this requires that the Rh atoms are low coordinated and geometrically unshielded by the Al atoms. Indeed, the most reactive Al_nRh^+ (n = 1 to 3, and 7) and $Al_nRh_2^+$ (n = 1 to 4 and 7) clusters contain low-coordinated and relatively unshielded Rh atoms. Such a dopant content enhanced reactivity toward hydrogen adsorption has also been observed for vanadium and cobalt doped aluminum clusters.[14,15,31] For both the singly and doubly Rh doped clusters, the initial molecular adsorption of H_2 is identified as the key step for the hydrogenation of Al_nRh^+ (n = 1 to 12) and $Al_nRh_2^+$ (n = 1 to 9) clusters. In addition, the geometrically easily accessible Rh centers with lower coordination are the preferred reactive sites for initial molecular hydrogen adsorption and contribute mainly to the size-dependent cluster reactivity. For singly Rh doped Al_nRh^+, molecular H_2 adsorption is favorable for sizes n = 2 and 3, while dissociative H_2 adsorption is preferred for other sizes. For doubly Rh doped $Al_nRh_2^+$, dissociative H_2 adsorption is only reachable for sizes n = 1, 2, and 7, while H_2 adsorbs molecularly for n = 3 to 6, 8, and 9, either due to energetic preferences (n = 3 and 4) or considerable energy barriers involved in the processes of H_2 dissociation (n = 5, 6, and 8) and the approaching of H_2 toward the cluster (n = 9).

5. CONCLUSION

The gas-phase interaction of H_2 with $Al_nRh_2^+$ (n = 1 to 9) was investigated by a combination of mass spectrometry, IRMPD spectroscopy, and DFT calculations. A strongly size-dependent reactivity of $Al_nRh_2^+$ toward H_2 was found, both experimentally and theoretically. DFT calculations indicate that the position and the coordination numbers of the Rh atoms are the main determinants for the initial molecular H_2 adsorption. The most reactive $Al_nRh_2^+$ (n = 1 to 4 and 7) contain accessible Rh atoms with low coordination, while the Rh atoms of the less reactive sizes (n = 5, 6, 8, and 9) are highly coordinated and at least one of them is geometrically shielded to thus hinder H_2 adsorption. Besides, the natural charge distributions of the Rh atoms as well as the charge transfer between $Al_nRh_2^+$ and H_2 contribute to the size-dependent reactivity of the clusters. In our previous work on singly Rh doped Al_nRh^+ (n = 1 to 12) clusters, dissociative H_2 adsorption was identified for the majority of the studied sizes (n = 1, 4 to 12), while molecular H_2 adsorption is only favorable for small sizes n = 2 and 3. In this work, however, dissociative H_2 adsorption is only reached for sizes n = 1, 2, and 7; while for n = 3 to 6, 8, and 9, molecular H_2 adsorption is preferred over dissociative adsorption, either due to energetic preferences (n = 3 and 4) or considerable energy barriers involved in the processes of H_2 dissociation (n = 5, 6, and 8) and the approaching of H_2 toward the cluster (n = 9). This investigation on the size-dependent reactivity of $Al_nRh_2^+$ (n = 1 to 9) clusters emphasizes the energy barriers involved in the H_2 interaction with the clusters and the effect of the Rh doping content on the hydrogen capacity. Both of them are vital issues involved in hydrogen storage with respect to molecular or dissociative hydrogen adsorption.

■ ASSOCIATED CONTENT

Supporting Information

The Supporting Information is available free of charge at https://pubs.acs.org/doi/10.1021/acs.jpcc.9b11230.

Computational results: (1) comparisons of the IRMPD spectra for $Al_2Rh_2H_{2m}^+$ (m = 3 and 4), $Al_nRh_2H_4^+$ (n = 3 and 4), and $Al_nRh_2H_2^+$ (n = 4, 7, and 8) with the PBE/Def2-TZVP calculated harmonic IR spectra of several low energy isomers; (2) PBE/Def2-TZVP calculated low energy isomers for $Al_nRh_2^+$, $Al_nRh_2{\cdot}H_2^+$, and $Al_nRh_2H_2^+$ (n

https://dx.doi.org/10.1021/acs.jpcc.9b11230
J. Phys. Chem. C 2020, 124, 7624−7633

= 1 to 9); (3) PBE(GD3BJ)/Def2-TZVP calculated energy profiles for single H_2 adsorption and dissociation on $Al_nRh_2^+$ (n = 3 to 8), the intrinsic reaction coordinates, and potential energy curves for reactions of $Al_nRh_2^+$ (n = 1 to 8) with H_2, as well as the PBE/Def2-TZVP calculated energy profile for $Al_9Rh_2{\cdot}H_2^+$ when the molecularly adsorbed H_2 approaches the Rh adsorption site; (4) PBE/Def2-TZVP calculated low energy isomers for $Al_nRh_2H_{2m}^+$ (n = 1 to 9) and the multiple hydrogen adsorption energies for n = 1 to 3; (5) correlations of the total abundances of the hydrogenated $Al_nRh_2H_{2m}^+$ (n = 1 to 9) clusters with PBE/Def2-TZVP calculated total NPA charges on the two Rh atoms, vertical electron affinities, and vertical ionization energies of $Al_nRh_2^+$ (n = 1 to 9) (PDF)

AUTHOR INFORMATION

Corresponding Author

Ewald Janssens − *Quantum Solid-State Physics, Department of Physics and Astronomy, KU Leuven, 3001 Leuven, Belgium;* orcid.org/0000-0002-5945-1194; Phone: +32 16 32 72 07; Email: ewald.janssens@kuleuven.be

Authors

Meiye Jia − *Quantum Solid-State Physics, Department of Physics and Astronomy, KU Leuven, 3001 Leuven, Belgium;* orcid.org/0000-0002-1407-1171

Jan Vanbuel − *Quantum Solid-State Physics, Department of Physics and Astronomy, KU Leuven, 3001 Leuven, Belgium*

Piero Ferrari − *Quantum Solid-State Physics, Department of Physics and Astronomy, KU Leuven, 3001 Leuven, Belgium;* orcid.org/0000-0001-6096-7772

Wieland Schöllkopf − *Fritz-Haber-Institut der Max-Planck-Gesellschaft, 14195 Berlin, Germany;* orcid.org/0000-0003-0564-203X

André Fielicke − *Fritz-Haber-Institut der Max-Planck-Gesellschaft, 14195 Berlin, Germany;* orcid.org/0000-0003-0400-0932

Minh Tho Nguyen − *Department of Chemistry, KU Leuven, 3001 Leuven, Belgium;* orcid.org/0000-0002-3803-0569

Complete contact information is available at: https://pubs.acs.org/10.1021/acs.jpcc.9b11230

Notes

The authors declare no competing financial interest.

ACKNOWLEDGMENTS

This work is supported by the KU Leuven Research Council (C14/18/073). J.V. and P.F. thank the Research Foundation Flanders (FWO) for a PhD and a postdoctoral fellowship, respectively.

REFERENCES

(1) Schlapbach, L.; Züttel, A. Hydrogen-Storage Materials for Mobile Applications. *Nature* **2001**, *414*, 353−358.

(2) Kubas, G. J. Fundamentals of H_2 Binding and Reactivity on Transition Metals Underlying Hydrogenase Function and H_2 Production and Storage. *Chem. Rev.* **2007**, *107*, 4152−4205.

(3) Zhou, L. Progress and Problems in Hydrogen Storage Methods. *Renewable Sustainable Energy Rev.* **2005**, *9*, 395−408.

(4) Sakintuna, B.; Lamaridarkrim, F.; Hirscher, M. Metal Hydride Materials for Solid Hydrogen Storage: A Review. *Int. J. Hydrogen Energy* **2007**, *32*, 1121−1140.

(5) Orimo, S.-i.; Nakamori, Y.; Eliseo, J. R.; Züttel, A.; Jensen, C. M. Complex Hydrides for Hydrogen Storage. *Chem. Rev.* **2007**, *107*, 4111−4132.

(6) Eberle, U.; Felderhoff, M.; Schüth, F. Chemical and Physical Solutions for Hydrogen Storage. *Angew. Chem., Int. Ed.* **2009**, *48*, 6608−6630.

(7) Goodman, D. W.; Kelley, R. D.; Madey, T. E.; Yates, J. T. Kinetics of the Hydrogenation of CO over a Single-Crystal Nickel-Catalyst. *J. Catal.* **1980**, *63*, 226−234.

(8) Zhang, F.; Wang, Y.; Chou, M. Y. Hydrogen Interaction with the Al Surface Promoted by Subsurface Alloying with Transition Metals. *J. Phys. Chem. C* **2012**, *116*, 18663−18668.

(9) Kobayashi, H.; Morita, H.; Yamauchi, M.; Ikeda, R.; Kitagawa, H.; Kubota, Y.; Kato, K.; Takata, M. Nanosize-Induced Hydrogen Storage and Capacity Control in a Non-Hydride-Forming Element: Rhodium. *J. Am. Chem. Soc.* **2011**, *133*, 11034−11037.

(10) Chopra, I. S.; Chaudhuri, S.; Veyan, J. F.; Chabal, Y. J. Turning Aluminium into a Noble-Metal-Like Catalyst for Low-Temperature Activation of Molecular Hydrogen. *Nat. Mater.* **2011**, *10*, 884−889.

(11) Swart, I.; de Groot, F. M. F.; Weckhuysen, B. M.; Gruene, P.; Meijer, G.; Fielicke, A. H_2 Adsorption on 3*d* Transition Metal Clusters: A Combined Infrared Spectroscopy and Density Functional Study. *J. Phys. Chem. A* **2008**, *112*, 1139−1149.

(12) Swart, I.; Gruene, P.; Fielicke, A.; Meijer, G.; Weckhuysen, B. M.; de Groot, F. M. F. Molecular Adsorption of H_2 on Small Cationic Nickel Clusters. *Phys. Chem. Chem. Phys.* **2008**, *10*, 5743−5745.

(13) Pino, I.; Kroes, G. J.; van Hemert, M. C. Hydrogen Dissociation on Small Aluminum Clusters. *J. Chem. Phys.* **2010**, *133*, 184304.

(14) Vanbuel, J.; Fernández, E. M.; Ferrari, P.; Gewinner, S.; Schöllkopf, W.; Balbás, L. C.; Fielicke, A.; Janssens, E. Hydrogen Chemisorption on Singly Vanadium-Doped Aluminum Clusters. *Chem. - Eur. J.* **2017**, *23*, 15638−15643.

(15) Nonose, S.; Sone, Y.; Onodera, K.; Sudo, S.; Kaya, K. Reactivity Study of Alloy Clusters Made of Aluminum and Some Transition-Metals with Hydrogen. *Chem. Phys. Lett.* **1989**, *164*, 427−432.

(16) Henry, D. J.; Yarovsky, I. Dissociative Adsorption of Hydrogen Molecule on Aluminum Clusters: Effect of Charge and Doping. *J. Phys. Chem. A* **2009**, *113*, 2565−2571.

(17) Wang, L.; Zhao, J.; Zhou, Z.; Zhang, S. B.; Chen, Z. First-Principles Study of Molecular Hydrogen Dissociation on Doped $Al_{12}X$ (X = B, Al, C, Si, P, Mg, and Ca) Clusters. *J. Comput. Chem.* **2009**, *30*, 2509−2514.

(18) Charkin, O. P.; Mikhailin, A. A.; Klimenko, N. M. Theoretical Modeling of Elementary Reactions of Dissociative Addition of an H_2 Molecule to Aluminum Clusters MAl_{12} Doped with Early 3*d* and 4*d* Transition Metal Atoms. *Russ. J. Inorg. Chem.* **2013**, *58*, 1479−1488.

(19) Guo, L. First-Principles Study of Molecular Hydrogen Adsorption and Dissociation on Al_nCr (n = 1−13) Clusters. *J. Phys. Chem. A* **2013**, *117*, 3458−3466.

(20) Bowker, M. Automotive Catalysis Studied by Surface Science. *Chem. Soc. Rev.* **2008**, *37*, 2204−2211.

(21) Inderwildi, O. R.; Jenkins, S. J.; King, D. A. Dynamic Interplay between Diffusion and Reaction: Nitrogen Recombination on Rh{211} in Car Exhaust Catalysis. *J. Am. Chem. Soc.* **2008**, *130*, 2213−2220.

(22) Roy, S.; Hegde, M. S.; Sharma, S.; Lalla, N. P.; Marimuthu, A.; Madras, G. Low Temperature NO_x and N_2O Reduction by H_2: Mechanism and Development of New Nano-Catalysts. *Appl. Catal., B* **2008**, *84*, 341−350.

(23) Duś, R.; Nowicka, E.; Nowakowski, R. Hydrogen Adsorption on Rhodium: Hydride Formed on the Surface of Thin Rhodium Films. *Appl. Surf. Sci.* **2008**, *254*, 4286−4291.

(24) Wang, X.; Andrews, L. Infrared Spectra of Rhodium Hydrides in Solid Argon, Neon, and Deuterium with Supporting Density Functional Calculations. *J. Phys. Chem. A* **2002**, *106*, 3706−3713.

(25) Mainardi, D. S.; Balbuena, P. B. Hydrogen and Oxygen Adsorption on Rh_n (n = 1−6) Clusters. *J. Phys. Chem. A* **2003**, *107*, 10370−10380.

(26) Bae, Y.-C.; Osanai, H.; Kumar, V.; Kawazoe, Y. Hydrogen Interaction on Rhodium Clusters. *Mater. Trans.* **2004**, *45*, 2587−2589.

(27) Ge, G. X.; Cao, H. B.; Jing, Q.; Luo, Y. H. Density Functional Theory Study of the Interaction of H_2 with Rhodium Clusters. *Sci. China, Ser. G: Phys., Mech. Astron.* **2009**, *58*, 8236−8242.
(28) Jia, M.; Vanbuel, J.; Ferrari, P.; Fernández, E. M.; Gewinner, S.; Schöllkopf, W.; Nguyen, M. T.; Fielicke, A.; Janssens, E. Size Dependent H_2 Adsorption on Al_nRh^+ (n = 1−12) Clusters. *J. Phys. Chem. C* **2018**, *122*, 18247−18255.
(29) Vanbuel, J.; Jia, M.; Ferrari, P.; Gewinner, S.; Schöllkopf, W.; Nguyen, M. T.; Fielicke, A.; Janssens, E. Competitive Molecular and Dissociative Hydrogen Chemisorption on Size Selected Doubly Rhodium Doped Aluminum Clusters. *Top. Catal.* **2018**, *61*, 62−70.
(30) Trivedi, R.; Bandyopadhyay, D. Study of Adsorption and Dissociation Pathway of H_2 Molecule on Mg_nRh (n = 1−10) Clusters: A First Principle Investigation. *Int. J. Hydrogen Energy* **2016**, *41*, 20113−20121.
(31) Vanbuel, J.; Fernández, E. M.; Jia, M.; Ferrari, P.; Schöllkopf, W.; Balbás, C.; Nguyen, M. T.; Fielicke, A.; Janssens, E. Hydrogen Chemisorption on Doubly Vanadium Doped Aluminum Clusters. *Z. Phys. Chem.* **2019**, *233*, 799−812.
(32) Chaudhuri, S.; Graetz, J.; Ignatov, A.; Reilly, J. J.; Muckerman, J. T. Understanding the Role of Ti in Reversible Hydrogen Storage as Sodium Alanate: A Combined Experimental and Density Functional Theoretical Approach. *J. Am. Chem. Soc.* **2006**, *128*, 11404−11415.
(33) Truong, N. X.; Haertelt, M.; Jaeger, B. K. A.; Gewinner, S.; Schöllkopf, W.; Fielicke, A.; Dopfer, O. Characterization of Neutral Boron-Silicon Clusters Using Infrared Spectroscopy: The Case of Si_6B. *Int. J. Mass Spectrom.* **2016**, *395*, 1−6.
(34) Schöllkopf, W.; Gewinner, S.; Junkes, H.; Paarmann, A.; von Helden, G.; Bluem, H.; Todd, A. M. M. The New IR and THz FEL Facility at the Fritz Haber Institute in Berlin. *Proc. SPIE* **2015**, *9512*, 95121L.
(35) Nesbitt, D. J.; Field, R. W. Vibrational Energy Flow in Highly Excited Molecules: Role of Intramolecular Vibrational Redistribution. *J. Phys. Chem.* **1996**, *100*, 12735−12756.
(36) Frisch, M. J.; Trucks, G. W.; Schlegel, H. B.; Scuseria, G. E.; Robb, M. A.; Cheeseman, J. R.; Scalmani, G.; Barone, V.; Mennucci, B.; Petersson, G. A., et al., *Gaussian 09*, Revision E.01., Gaussian, Inc., Wallingford CT, 2013.
(37) Perdew, J. P.; Burke, K.; Ernzerhof, M. Generalized Gradient Approximation Made Simple. *Phys. Rev. Lett.* **1996**, *77*, 3865−3868.
(38) Weigend, F.; Ahlrichs, R. Balanced Basis Sets of Split Valence, Triple Zeta Valence and Quadruple Zeta Valence Quality for H to Rn: Design and Assessment of Accuracy. *Phys. Chem. Chem. Phys.* **2005**, *7*, 3297−3305.
(39) Henry, D. J.; Varano, A.; Yarovsky, I. Performance of Numerical Basis Set DFT for Aluminum Clusters. *J. Phys. Chem. A* **2008**, *112*, 9835−9844.
(40) Wang, Y.; Lv, J.; Zhu, L.; Ma, Y. Crystal Structure Prediction Via Particle-Swarm Optimization. *Phys. Rev. B: Condens. Matter Mater. Phys.* **2010**, *82*, No. 094116.
(41) Lv, J.; Wang, Y.; Zhu, L.; Ma, Y. Particle-Swarm Structure Prediction on Clusters. *J. Chem. Phys.* **2012**, *137*, No. 084104.
(42) Grimme, S.; Ehrlich, S.; Goerigk, L. Effect of the Damping Function in Dispersion Corrected Density Functional Theory. *J. Comput. Chem.* **2011**, *32*, 1456−1465.
(43) Schlegel, H. B. Optimization of Equilibrium Geometries and Transition Structures. *J. Comput. Chem.* **1982**, *3*, 214−218.
(44) Gonzalez, C.; Schlegel, H. B. Reaction Path Following in Mass-Weighted Internal Coordinates. *J. Chem. Phys.* **1989**, *90*, 2154−2161.
(45) Frisch, M. J.; Trucks, G. W.; Schlegel, H. B.; Scuseria, G. E.; Robb, M. A.; Cheeseman, J. R.; Scalmani, G.; Barone, V.; Mennucci, B.; Petersson, G. A., et al., *Gaussian 16*, Revision B.01., Gaussian, Inc., Wallingford CT, 2016.
(46) Calvo, F.; Li, Y.; Kiawi, D. M.; Bakker, J. M.; Parneix, P.; Janssens, E. Nonlinear Effects in Infrared Action Spectroscopy of Silicon and Vanadium Oxide Clusters: Experiment and Kinetic Modeling. *Phys. Chem. Chem. Phys.* **2015**, *17*, 25956−25967.
(47) Jia, M. Y.; Xu, B.; Ding, X. L.; He, S. G.; Ge, M. F. Experimental and Theoretical Study of the Reactions between Manganese Oxide Cluster Anions and Hydrogen Sulfide. *J. Phys. Chem. C* **2012**, *116*, 24184−24192.
(48) Huber, K. P.; Herzberg, G. *Molecular Spectra and Molecular Structure: IV. Constants of Diatomic Molecules*; Springer: New York, 2013.
(49) Conceicao, J.; Laaksonen, R. T.; Wang, L. S.; Guo, T.; Nordlander, P.; Smalley, R. E. Photoelectron Spectroscopy of Transition-Metal Clusters: Correlation of Valence Electronic Structure to Reactivity. *Phys. Rev. B: Condens. Matter Mater. Phys.* **1995**, *51*, 4668−4671.
(50) Whetten, R. L.; Cox, D. M.; Trevor, D. J.; Kaldor, A. Correspondence between Electron Binding Energy and Chemisorption Reactivity of Iron Clusters. *Phys. Rev. Lett.* **1985**, *54*, 1494−1497.
(51) Elkind, J. L.; Weiss, F. D.; Alford, J. M.; Laaksonen, R. T.; Smalley, R. E. Fourier Transform Ion Cyclotron Resonance Studies of H_2 Chemisorption on Niobium Cluster Cations. *J. Chem. Phys.* **1988**, *88*, 5215−5224.
(52) Burkart, S.; Blessing, N.; Gantefor, G. Indication of a Size-Dependent Transition from Molecular to Dissociative Chemisorption on Clusters. *Phys. Rev. B: Condens. Matter Mater. Phys.* **1999**, *60*, 15639−15642.
(53) Knickelbein, M. B. Reactions of Transition Metal Clusters with Small Molecules. *Annu. Rev. Phys. Chem.* **1999**, *50*, 79−115.

https://dx.doi.org/10.1021/acs.jpcc.9b11230
J. Phys. Chem. C 2020, 124, 7624−7633